Photoexcitation of ^{76}Ge

R. Schwengner,[1,*] R. Massarczyk,[2] K. Schmidt,[1] K. Zuber,[3] R. Beyer,[1] D. Bemmerer,[1] S. Hammer,[1] A. Hartmann,[1] T. Hensel,[1,3] H. F. Hoffmann,[1,3] A. R. Junghans,[1] T. Kögler,[1,4] S. E. Müller,[1] M. Pichotta,[3] S. Turkat,[3] J. A. B. Turko,[1,4] S. Urlaß,[1,5] and A. Wagner[1]

[1]*Helmholtz-Zentrum Dresden-Rossendorf, 01328 Dresden, Germany*
[2]*Los Alamos National Laboratory, Los Alamos, New Mexico 87545, USA*
[3]*Institut für Kern- und Teilchenphysik, Technische Universität Dresden, 01069 Dresden, Germany*
[4]*OncoRay, National Center for Radiation Research in Oncology, Faculty of Medicine and University Hospital Carl Gustav Carus, Technische Universität Dresden, 01309 Dresden, Helmholtz-Zentrum Dresden-Rossendorf, 01328 Dresden, Germany*
[5]*Conseil Européen pour la Recherche Nucléaire (CERN), 1211 Meyrin, Geneva, Switzerland*

(Received 15 June 2021; revised 8 September 2021; accepted 21 January 2022; published 4 February 2022)

The dipole strength of the nuclide ^{76}Ge was studied in photon-scattering experiments using bremsstrahlung produced with electron beams of energies of 7.8 and 12.3 MeV delivered by the electron linear accelerator of high brilliance and high brightness (ELBE). We identified 210 levels up to an excitation energy of 9.4 MeV and assigned spin $J = 1$ to most of them. The quasicontinuum of unresolved transitions was included in the analysis of the spectra and the intensities of branching transitions were estimated on the basis of simulations of statistical γ-ray cascades. The photoabsorption cross section up to the neutron-separation energy was determined and is compared with predictions of the statistical reaction model. The derived photon strength function is compared with results of experiments using other reactions.

DOI: 10.1103/PhysRevC.105.024303

I. INTRODUCTION

The search for signals of the neutrinoless double-β ($0\nu\beta\beta$) decay is currently one of the most challenging experimental efforts expected to gain information about the validity of the standard model of particle physics. The existence of this decay mode would imply that neutrinos are identical with antineutrinos, their antiparticles, and that special conditions for their vertices exist, realized, for example, through a nonzero neutrino mass [1]. The discovery of this process would prove that the lepton number is violated by two units and thus that physics goes beyond the standard model. Experiments searching for this very rare decay mode need large amounts of target material under very low background conditions. Hence, the experiments are performed deep underground. Among the nuclides, where $\beta\beta$ decay is possible in contrast to β decay, there is the nuclide ^{76}Ge, which can be used at the same time as target and detector material. Collaborations using this target and detector material are, for example, MAJORANA [2] and GERDA [3]. Up to now, GERDA is the experiment that sets the strongest limit on the half-life of the $0\nu\beta\beta$ decay of ^{76}Ge to about 10^{26} years [4]. The next generation of experiments, such as LEGEND [5], tries to reach 10^{28} years. Thus, lower background levels have to be reached and every possible background reaction channel has to be understood as well as possible. Another current project is CDEX-1 [6]. If the $0\nu\beta\beta$ decay is realized in nature, the β spectrum is discrete rather than continuous. The signal for this process is a peak at the Q value of (2039.006 ± 0.050) keV in the sum-energy spectrum.

An important issue for this search is the exclusion of signals from other reactions on ^{76}Ge that involve the emission of γ rays of about this energy. Earlier experiments using the ^{76}Ge(n,γ) reaction revealed a γ ray at 2035.5 keV [7]. A 2040.7-keV γ ray was identified in the β decay of ^{76}Ga [8]. In ^{76}Ge$(n,n'\gamma)$ experiments, γ rays at 2034.8 [9] and 2038.9 keV [10] were observed. Various experiments using neutron-induced reactions or activations on Ge isotopes are currently performed at several laboratories. In addition to these, one may think of other reactions that can serve to identify so far unknown γ transitions in ^{76}Ge. One of these reactions is photon scattering (γ,γ'), also called nuclear resonance fluorescence, in which the incident photons transfer preferentially angular momentum $L = 1$ and hence excite states of spin $J = 1$ from the ground state in even-even nuclei. In the present work, we performed photon-scattering experiments at the bremsstrahlung facility γELBE [11] of Helmholtz-Zentrum Dresden-Rossendorf (HZDR) to study states up to the neutron-separation energy $S_n = 9.4$ MeV and their deexcitation to low-lying states, in particular the possible occurrence of γ rays with energies in the interesting region around 2039 keV.

In addition to the just described interest from the search for the $0\nu\beta\beta$ decay of ^{76}Ge, photon scattering from ^{76}Ge is also of interest for nuclear structure and reaction physics. Photoabsorption cross sections σ_γ and the related photon strength

*r.schwengner@hzdr.de

functions $f_1(E_\gamma)$ for $L = 1$ have attracted growing interest [12,13] because of their importance as inputs to calculations of reaction cross sections within the statistical reaction model [14]. In photoabsorption, the two quantities are connected via the relation $\sigma_\gamma = g(\pi\hbar c)^2\ E_\gamma\ f_1(E_\gamma)$ with $g = (2J_x + 1)/(2J_0 + 1)$, where J_x and J_0 are the spins of the excited and ground states, respectively. It was shown, for example, that the so-called pygmy dipole resonance (PDR) [15–17], an extra strength found on top of the tail of the isovector giant dipole resonance (GDR), influences neutron-capture reaction rates [18,19], which are important for the synthesis of heavy elements in astrophysical processes [20,21].

In an earlier photon-scattering experiment on ^{76}Ge using unpolarized bremsstrahlung at the former Stuttgart Dynamitron and polarized bremsstrahlung at the former Gießen linear accelerator, 30 states with $J = 1$ were identified between 2.9 and 9.1 MeV and parities were assigned to 17 of them [22]. Further experiments were performed using bremsstrahlung at the S-Dalinac electron accelerator of Technische Universität Darmstadt, Germany [23], and quasimonoenergetic, polarized photons at the high-intensity γ-ray source (HIγS) [24] of the Triangle Universities Nuclear Laboratory (TUNL) in Durham, North Carolina, USA. The experiments are briefly described in Ref. [25] while 128 states with 1^- assignments and 2 with 1^+ assignments between 4.4 and 8.9 MeV are compiled in a Ph.D. thesis [26]. In the present work, we found 210 states and assigned $J = 1$ to most of them. In addition, we determined the photon-scattering cross section for 10 keV bins of excitation energy up to S_n. In this analysis, the intensity in the quasicontinuum part of the spectrum was taken into account. Moreover, we estimated average intensities of inelastic transitions to low-lying excited states and branching ratios of the ground-state transitions by means of simulations of statistical γ-ray cascades. Using these quantities, we determined the photoabsorption cross section.

Photon strength functions in ^{76}Ge have previously been studied using β decay of ^{76}Ga in connection with the so-called Oslo method [27]. Preliminary results for a photon strength function deduced from photon-scattering experiments with quasimonoenergetic photons at HIγS were presented in Ref. [28].

II. EXPERIMENTAL METHODS AND RESULTS

A. The photon-scattering method

In photon-scattering experiments, the energy- and solid-angle-integrated scattering cross section I_s of an excited state at the energy E_x is deduced from the measured intensity of the respective transition to the ground state. It can be determined relative to known integrated scattering cross sections. In the present experiments, we used the integrated scattering cross sections $I_s(E_x^{\rm B})$ of states in ^{11}B [29] and their angular correlations including mixing ratios [30] as a reference:

$$\frac{I_s(E_x)}{I_s(E_x^{\rm B})} = \left(\frac{I_\gamma(E_\gamma,\theta)}{W(E_\gamma,\theta)\Phi_\gamma(E_x)N_N}\right) \times \left(\frac{I_\gamma(E_\gamma^{\rm B},\theta)}{W(E_\gamma^{\rm B},\theta)\Phi_\gamma(E_x^{\rm B})N_N^{\rm B}}\right)^{-1}. \quad (1)$$

Here, $I_\gamma(E_\gamma,\theta)$ and $I_\gamma(E_\gamma^{\rm B},\theta)$ denote the efficiency-corrected measured intensities of a considered ground-state transition at energy E_γ and of a ground-state transition in ^{11}B at $E_\gamma^{\rm B}$, respectively, observed at an angle θ to the beam. $W(E_\gamma,\theta)$ and $W(E_\gamma^{\rm B},\theta)$ describe the angular correlations of these transitions. The quantities N_N and $N_N^{\rm B}$ are the areal densities of nuclei in the ^{76}Ge and ^{11}B targets, respectively. The quantities $\Phi_\gamma(E_x)$ and $\Phi_\gamma(E_x^{\rm B})$ stand for the photon fluxes at the energy of the considered level and at the energy of a level in ^{11}B, respectively.

The integrated scattering cross section is related to the partial width of the ground-state transition Γ_0 according to

$$I_s = \int_0^{+\infty}\sigma_{\gamma\gamma}\,dE = \left(\frac{\pi\hbar c}{E_x}\right)^2 \frac{2J_x+1}{2J_0+1}\frac{\Gamma_0^2}{\Gamma}, \quad (2)$$

where $\sigma_{\gamma\gamma}$ is the elastic scattering cross section; E_x, J_x, and Γ denote energy, spin, and total width of the excited level, respectively; and J_0 is the spin of the ground state. If a given level deexcites to low-lying excited states (inelastic scattering) in addition to the deexcitation to the ground state (elastic scattering), then the branching ratio $b_0 = \Gamma_0/\Gamma$ of the ground-state transition has to be known to deduce Γ_0. The γ-ray intensities and, hence, the deduced quantities I_s and Γ_0 are also distorted if a level is populated from higher lying levels. This feeding can be reduced by choosing beam energies not far above the considered levels.

Spins of excited states are deduced by comparing experimental ratios of γ-ray intensities, measured at two angles, with theoretical predictions. The optimum combination includes angles of 90° and 127° to the beam direction, because the respective ratios for the spin sequences 0-1-0 and 0-2-0 differ most at these angles. The expected values are $W(90^\circ)/W(127^\circ)_{0\text{-}1\text{-}0} = 0.74$ and $W(90^\circ)/W(127^\circ)_{0\text{-}2\text{-}0} = 2.15$ by taking into account opening angles of 16° and 14° of the collimators in front of the detectors placed at 90° and 127°, respectively, in the setup at γELBE [11].

B. The target

The target consisted of 1.8760 g of germanium, enriched to 93.4% in ^{76}Ge, in a square shape of 15 mm × 11 mm. The germanium target was combined with 0.300 g of boron, enriched to 99.5% in ^{11}B and formed to a disk of 20 mm in diameter. The known integrated scattering cross sections of levels in ^{11}B were used to determine the photon flux (see Sec. II D). The photon-flux density was proven to be nearly constant in a spot of about 25 mm in diameter [31]. For the calculation of cross sections for ^{76}Ge, the ratio of the ^{76}Ge and ^{11}B target areas was taken into account.

C. Detector response

For the determination of the integrated scattering cross sections according to Eq. (1), the relative efficiencies of the detectors and the photon flux are needed. The detector response was simulated using the program package GEANT4 [32–34]. The reliability of the simulations was tested by comparing simulated spectra with measured ones as described, for example, in Refs. [31,35–38]. The determination of the absorption cross section requires in addition a correction of the experimental spectra for photons scattered by atomic processes induced by the impinging photons in the target material, and for ambient background radiation, which is described in Sec. III.

The absolute efficiencies of the high-purity germanium (HPGe) detectors in the setup at γELBE were determined experimentally up to 2.4 MeV from measurements with a ^{226}Ra calibration source. For interpolation, an efficiency curve calculated with GEANT4 and scaled to the absolute experimental values was used. A check of the simulated efficiency curve up to about 9 MeV was performed via various (p,γ) reactions at the HZDR Tandetron accelerator. The efficiency values deduced from these measurements agree with the simulated values within their uncertainties [39]. Similar results were obtained for the resonances at 4.44 and 11.66 MeV in ^{12}C populated in the ^{11}B(p,γ) reaction at the van de Graaff accelerator of the Triangle Universities Nuclear Laboratory (TUNL) in Durham, North Carolina, USA [40].

D. Experiments and results

The nuclide ^{76}Ge was studied in two experiments at γELBE [11]. Bremsstrahlung was produced using electron beams of 7.8 and 12.3 MeV kinetic energy, respectively. In the measurement at 7.8 MeV, the electron beam hit a niobium foil of 7 μm thickness acting as a radiator at an average current of about 700 μA. In the measurement at 12.3 MeV, the niobium foil had a thickness of 12.5 μm and the average current was also about 700 μA. A 10-cm-thick aluminum absorber (beam hardener) was placed behind the radiator to reduce the low-energy intensity of the bremsstrahlung spectrum in the measurement at 12.3 MeV. The photon beam was collimated by a 260-cm-long pure aluminum collimator with a conical borehole of 8 mm in diameter at the entrance, 90 cm behind the radiator, and 24 mm in diameter at the exit. The target, placed 200 cm behind the collimator exit, was irradiated with a typical flux of about 10^9 s^{-1} in a spot of 38 mm in diameter. Scattered photons were measured with four HPGe detectors with a full-energy efficiency of 100% relative to a NaI detector of 7.6 cm in diameter and 7.6 cm in length. All HPGe detectors were surrounded by escape-suppression shields made of bismuth germanate (BGO) scintillation detectors 3 cm in thickness. Two HPGe detectors were placed vertically at 127° relative to the photon-beam direction and a distance of 32 cm from the target. The other two HPGe detectors were positioned in a horizontal plane at 90° to the beam and a distance of 28 cm from the target. Absorbers of 8 mm Pb plus 3 mm Cu were placed in front of the detectors at 90° and of 3 mm Pb plus 3 mm Cu in front of the detectors at 127°. Spectra of scattered photons were measured for 132 h each in the experiments at 7.8 and 12.3 MeV electron energy. Part of a spectrum including events measured with the two detectors placed at 127° relative to the beam at an electron energy of 12.3 MeV is shown in Fig. 1.

The absolute photon fluxes in the two measurements at γELBE were determined from intensities and known integrated scattering cross sections of transitions in ^{11}B. The 7283-keV transition in ^{11}B was found to form an unresolved doublet with another transition, which is negligible at $E_e = 7.8$ MeV, but comparable in intensity with the transition in ^{11}B at $E_e = 12.3$ MeV. The latter has therefore not been considered for the flux determination. For interpolation, the photon flux was calculated using a bremsstrahlung computer code [41] based on the Born approximation with Coulomb correction [42] and including an atomic screening correction [43]. In addition, the flux was corrected for the attenuation by the beam hardener by applying a parametrization of the results

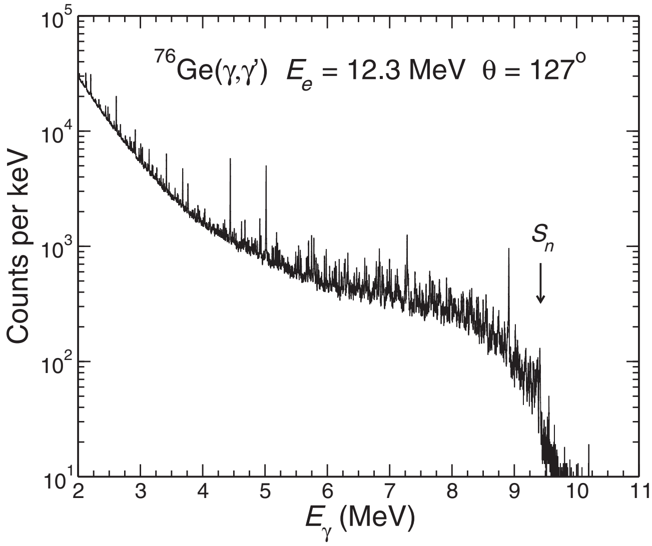

FIG. 1. Part of a spectrum of photons scattered from ^{76}Ge combined with ^{11}B, measured during the irradiation with bremsstrahlung produced by electrons of an energy of $E_e^{\mathrm{kin}} = 12.3$ MeV. This spectrum is the sum of the spectra measured with the two detectors placed at 127° relative to the beam at γELBE. The arrow labeled S_n indicates the neutron-separation energy.

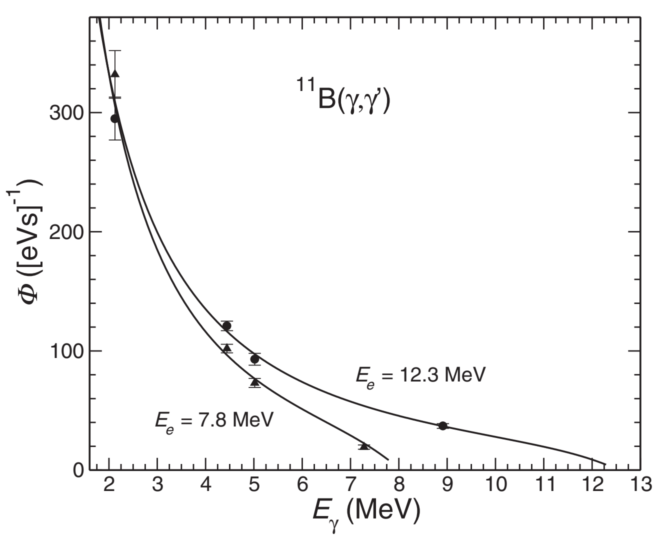

FIG. 2. Average absolute photon flux on the ^{11}B target deduced from intensities of known transitions in ^{11}B for the measurements at $E_e = 7.8$ MeV (triangles) and $E_e = 12.3$ MeV (circles) at γELBE. The curves represent the calculated flux described in the text.

TABLE I. Levels assigned to ^{76}Ge.

E_x (keV)[a]	$I_\gamma(90^\circ)\,/\,I_\gamma(127^\circ)$[b]	J_x^π[c]	I_s (eV b)[d]
564.5(1)	1.05(14)	2^+[e]	
1109.2(1)	1.11(15)	2^+[e]	
2504.2(4)		2^+[e]	
2655.1(3)	0.79(27)	(1)	5.6(10)
2919.3(2)	1.33(24)	1^+[e]	12.1(12)
3006.7(2)	0.90(16)	1^+[e]	9.6(10)
3140.9(2)	1.05(15)	1^+[e]	12.0(12)
3200.0(2)	1.23(23)		9.7(11)
3418.9(1)	0.86(4)	1^+[f]	46(4)
3680.4(1)	0.84(3)	1^-[f]	52(4)
3763.2(1)	0.83(6)	1^+[f]	25.8(24)
3951.0(4)	1.10(28)		4.5(7)
4024.0(2)	0.70(20)	$1^{(-)}$[f]	6.2(8)
4035.0(2)	0.76(15)	1	9.1(10)
4115.9(2)	0.81(12)	1	14.7(16)
4250.8(3)	0.68(20)	1	6.7(11)
4624.0(2)	0.84(8)	1^+[f]	26.9(24)
4661.0(4)	0.53(16)	1	6.4(10)
4678.1(1)	0.75(5)	1	33.0(28)
4722.2(2)	0.88(15)	(1)	9.6(12)
4741.0(2)	0.94(15)		10.3(12)
4788.9(3)	1.17(26)		7.1(11)
4837.0(4)	0.88(20)	(1)	7.3(12)
4845.9(3)	0.76(13)	1	10.9(13)
4874.5(2)	1.5(6)		8.7(13)
4916.5(1)	0.75(4)	1	50(4)
4935.9(2)	0.91(7)	1	19.5(18)
5116.4(2)	0.85(9)	1	17.3(18)
5166.7(2)	0.91(9)	(1)	17.3(16)
5185.8(1)	0.98(6)	(1)	38(3)
5202.3(2)	0.80(8)	1	22.3(20)
5222.0(3)	1.04(15)		13.3(16)
5266.8(3)	0.65(13)	1	11.6(16)
5273.6(6)	0.80(24)	(1)	5.0(10)
5284.9(2)	0.60(10)	1	13.1(15)
5304.1(3)	0.56(13)	1	10.2(13)
5365.6(3)	0.68(12)	1	10.1(13)
5379.5(4)	0.59(16)	1	6.2(10)
5390.6(5)	0.81(22)	(1)	5.4(10)
5418.6(4)	0.76(27)	(1)	5.4(10)
5434.3(3)	0.74(22)	1	7.9(11)
5492.7(2)	0.62(13)	1	21.3(25)
5540.1(2)	0.76(5)	1	31.6(27)
5567.4(2)	0.92(8)	(1)	20.6(19)
5581.0(2)	0.66(8)	1	16.0(16)
5665.2(3)	0.72(10)	1	20.8(24)
5677.6(3)	0.75(11)	1	23.5(26)
5698.8(2)	0.74(6)	1^-[f]	52(5)
5708.4(6)	0.98(21)	(1)	8.3(14)
5748.3(1)	0.81(5)	1^-[f]	67(5)
5785.0(2)	0.72(5)	1	52(4)
5794.1(2)	0.66(7)	1	26.5(25)
5820.8(6)			22(5)
5825.3(8)	0.76(10)	1	12(3)
5846.5(7)	0.81(28)		8.8(21)
5864.8(6)	0.83(22)		10.8(22)
5908.8(3)			8.1(13)
5954.8(2)	0.71(5)	1	41(3)
5983.0(2)	0.69(4)	1^-[f]	49(4)
6048.4(4)	0.81(20)	1	7.8(13)
6081.4(4)	0.90(16)	(1)	12.4(17)
6102.0(9)			5.3(12)
6113.6(3)	0.77(9)	1	21.1(22)
6130.3(2)	0.76(7)	1	30.9(29)
6145.6(2)	0.77(9)	1	24.2(25)
6162.4(9)	0.9(4)		4.5(14)
6191.3(2)	0.72(6)	1	41(4)
6223.4(7)			6.0(14)
6228.2(4)	0.79(11)	1	14.5(20)
6234.8(9)			4.6(12)
6240.7(3)	0.70(14)	1	13.3(18)
6272.7(3)	0.79(9)	1	24.0(25)
6285.3(2)	0.68(6)	1	46(4)
6315.4(4)	0.66(11)	1	21.5(26)
6330.2(2)	0.77(5)	1	63(5)
6366.2(11)	1.0(3)		8.7(21)
6393.2(5)	0.81(19)	1	15.5(26)
6408.1(5)	0.63(29)	1	17(3)
6436.1(9)	1.2(4)		12.0(28)
6448.3(11)	0.9(4)		8.2(23)
6472.2(3)	0.79(9)	1	41(4)
6497.9(3)	0.72(13)	1	18.7(27)
6513.3(4)	0.75(11)	1	31(4)
6572.0(6)	1.08(21)		11.8(18)
6601.2(2)	0.77(6)	1	53(5)
6611.1(6)			13.0(19)
6629.0(3)	0.79(9)	1	27.0(28)
6641.9(5)	1.00(15)		16.5(21)
6661.4(9)			9.6(19)
6670.6(3)	0.85(9)	1	33(3)
6741.6(6)	0.86(20)	(1)	11.4(19)
6764.8(4)	0.74(11)	1	20.4(24)
6786.7(2)	0.83(6)	1	59(5)
6816.5(3)	0.75(7)	1	44(4)
6835.5(2)	0.70(5)	1	82(7)
6846.2(3)	0.66(7)	1	44(4)
6880.3(4)	0.70(6)	1	46(5)
6884.2(10)			18(2)
6898.9(5)	0.55(8)	1	41(6)
6908.0(18)	1.2(3)		19(5)
6938.6(7)	0.61(16)	1	15.1(27)
6959.9(3)	0.71(8)	1	45(5)
6985.1(5)	0.53(9)	1	26(3)
6998.7(3)	0.68(5)	1^-[f]	79(7)
7011.0(9)	0.46(16)	1	12.3(25)
7025.8(3)	0.73(8)	$1^{(-)}$[f]	51(5)
7047.9(9)	0.58(22)	1	10.4(26)
7081.2(9)	0.53(29)	1	9.0(22)
7091.4(4)	0.74(11)	1	28(3)
7102.4(6)	0.75(26)	1	13.8(24)
7121.3(3)	0.80(8)	1	42(4)
7130.1(3)	0.70(9)	1	36(4)

TABLE I. (*Continued.*)

E_x (keV)[a]	I_γ (90°) / I_γ (127°)[b]	J_x^{π} [c]	I_s (eV b)[d]
7147.3(4)	0.76(13)	1	23(3)
7171.6(9)			10.8(26)
7250.5(2)	0.79(8)	1^- [f]	76(7)
7289.7(4)	0.9(5)		51(5)
7300.7(3)	0.75(9)	1^- [f]	56(5)
7406.7(3)	0.76(11)	1	60(6)
7415.6(4)	0.98(18)		37(5)
7452.2(5)			24(4)
7478.6(5)	0.8(3)		21(3)
7485.0(3)	0.65(26)	1	33(4)
7521.2(5)	0.75(14)	1	26(4)
7536.6(4)	0.89(15)	(1)	30(4)
7548.8(7)	0.95(26)	(1)	19(4)
7584.6(4)	0.67(9)	1	46(5)
7642.6(4)	0.76(9)	1	69(7)
7650.8(4)	0.79(10)	1	58(6)
7677.7(4)	0.78(12)	1	44(5)
7694.0(3)	0.75(10)	1	59(7)
7722.7(4)	0.93(19)	(1)	36(6)
7776.9(7)	0.83(17)	(1)	28(5)
7783.8(9)			24(5)
7796.6(4)	0.70(10)	1	66(7)
7803.7(6)	0.76(13)	1	42(5)
7814.3(7)	0.79(16)	1	26(4)
7817.2(2)			20.7(17)
7836.3(6)			17(4)
7849.3(5)	0.77(24)	(1)	22(4)
7861.2(4)	0.51(20)	1	31(6)
7883.3(10)	0.69(26)	1	16(4)
7893.6(12)	1.0(4)		11(3)
7913.4(2)	0.80(7)	1	85(8)
7949.9(2)	0.86(12)	1	42(5)
7975.6(7)	0.93(16)	(1)	29(5)
7995.8(4)	0.85(18)	(1)	25(4)
8017.5(14)	0.7(3)	(1)	19(5)
8026.5(8)	0.86(25)	(1)	34(7)
8049.3(6)	0.82(21)	(1)	34(5)
8063.4(8)	0.71(27)	1	20(4)
8094.2(8)			12(4)
8102.8(5)	1.23(28)		24(5)
8109.5(8)			13(3)
8134.5(11)	1.4(5)		13(4)
8151.6(5)	0.85(12)	$1^{(-)}$ [f]	52(7)
8160.2(9)			25(5)
8177.8(4)	0.70(8)	1	56(6)
8187.8(5)	0.86(11)	1	49(6)
8236.4(4)	0.90(14)	(1)	44(6)
8252.9(9)			25(6)
8259.6(6)	0.86(16)	(1)	43(7)
8284.5(3)	0.88(13)	(1)	72(8)
8294.3(12)	0.86(25)		21(4)
8303.5(5)	0.77(13)	1	49(6)
8317.8(3)	0.74(9)	1	77(7)
8328.9(7)	0.77(15)	1	27(4)
8347.7(9)	0.84(25)		19(4)
8357.4(7)	0.91(29)	(1)	28(5)
8397.3(5)			38(6)
8418.0(15)			9(3)
8425.2(3)	1.18(26)		53(7)
8446.1(7)	0.5(4)	1	16(3)
8461.9(9)			13(3)
8500.0(3)	0.84(11)	1	62(7)
8520.7(6)			23(6)
8535.1(5)	0.61(20)	1	33(5)
8546.1(5)	0.68(11)	1^- [f]	73(10)
8552.3(8)	0.42(20)	1	34(7)
8566.9(3)	0.78(12)	1	49(6)
8602.3(5)			19(4)
8625.7(7)	0.49(25)	1	28(11)
8649.1(8)	1.20(28)		22(4)
8662.0(4)	0.89(12)	(1)	52(6)
8696.2(7)			20(10)
8740.7(4)	0.92(13)	(1)	41(5)
8752.8(4)	1.05(14)	1^- [f]	43(5)
8768.4(9)	0.62(25)	1	15(4)
8806.2(5)	1.2(5)		27(7)
8843.7(4)	0.67(11)	1	39(6)
8888.5(9)			19(5)
9014.2(14)		1^- [f]	24(9)
9019.5(10)	0.98(15)	(1)	37(12)
9033.1(9)	1.0(3)		15(4)
9051.7(12)	0.89(17)	(1)	17(5)
9058.5(11)	0.92(29)		18(5)
9163.3(9)	0.69(23)	1	13.9(28)
9175.5(8)	0.59(16)	1	19.1(29)
9187.4(4)	0.80(12)	1	35(4)
9254.6(7)	1.08(29)		21(4)
9264.1(6)	1.1(3)		22(3)
9305.0(4)			18.0(26)
9315.8(4)	1.0(5)		23(3)
9337.8(6)	1.0(3)		17(3)
9354.5(8)	0.92(29)	(1)	15.4(27)
9365.9(5)	0.81(18)	1	29(4)
9377.9(4)	0.95(18)	(1)	38(5)
9399.4(6)	0.60(17)	1	19(3)
9409.9(4)	0.69(11)	1	49(5)
9417.6(5)	0.52(13)	1	29(4)
9556.6(5)	0.71(22)	1	11.5(22)

[a]Excitation energy. The uncertainty of this and the other quantities in the table is given in parentheses in units of the last digit. This energy value was deduced from the γ-ray energy measured at 127° including a recoil and Doppler-shift correction.

[b]Ratio of the intensities measured at angles of 90° and 127°. The expected values for an elastic dipole transition (spin sequence 0-1-0) and for an elastic quadrupole transition (spin sequence 0-2-0) are 0.74 and 2.15, respectively.

[c]Spin deduced from the angular distribution of the ground-state transition. A tentative assignment of (1) is given, if the angular distribution is compatible with dipole as well as isotropic behavior.

[d]Energy-integrated scattering cross section. Below an excitation energy of 7.0 MeV the value was deduced from the measurement at 7.8 MeV electron energy, otherwise the value was deduced from the measurement at 12.3 MeV.

[e]Spin and parity taken from Ref. [10].

[f]Spin and parity taken from Ref. [22].

of a corresponding GEANT4 simulation. The calculated flux curves were adjusted to the experimental values obtained at the energies of levels in ^{11}B. The experimental flux values and the calculated curves are presented in Fig. 2.

The measurements at two electron energies allowed us to identify inelastic transitions that feed low-lying from high-lying levels. Transitions found in the measurement at $E_e^{\rm kin} =$ 7.8 MeV are assumed to be ground-state transitions. Additional transitions observed up to 7.8 MeV in the measurement at $E_e^{\rm kin} = 12.3$ MeV are considered to be inelastic transitions from high-lying to low-lying excited states. By comparing the respective spectra, these inelastic transitions were sorted out. Besides, there is a number of transitions with energies that fit the difference between the energy of a higher lying level and the first or second excited 2^+ states. These transitions are also assumed to be inelastic transitions, if their intensity is smaller than that of the ground-state transition from the considered higher lying level. The remaining ground-state transitions were used to derive the corresponding level energies, the integrated scattering cross sections of the states, and spin assignments deduced from angular distributions of the ground-state transitions. These quantities are compiled in Table I. The integrated scattering cross sections of levels up to $E_x = 7.0$ MeV were taken from the measurement at 7.8-MeV electron energy, because they are affected by feeding intensities in the 12.3-MeV measurement. We note that in principle low-lying states can also be fed from other states below 7.8 MeV. However, previous investigations have shown that the states below about 6 MeV are fed by states mainly above about 9 MeV [44,45].

A transition with an energy around 2039 keV, close to the one of the expected signal for the $0\nu\beta\beta$ decay, has not been clearly identified in the present experiments. In particular, the ground-state transition from the 3951-keV level, known from ^{76}Ga β decay [8], has been detected in the present study (see Table I), but there is no indication of the 2040-keV transition depopulating the 3951- to the 1911-keV levels in the measurement at $E_e = 7.8$ MeV. There may be a tiny bump in the measurement at $E_e = 12.3$ MeV, which occurs due to feeding of the 3951-keV level from higher lying levels. This situation is illustrated in Fig. 3. The tentative spin and parity assignment of $(1, 2^+)$ given in Ref. [8] for the 3951-keV level could not be made more precise because of the uncertain angular distribution of the weak ground-state transition. The spectrum at 12.3 MeV contains, for example, transitions from the 0_3^+ state at 2697 and from the 2_7^+ state at 3130 keV, which are not seen in the spectrum at 7.8 MeV. This proves that these low-lying states are mainly fed by states above about 8 MeV.

III. DETERMINATION OF THE DIPOLE-STRENGTH DISTRIBUTION

The determination of the dipole-strength distribution and the related photoabsorption cross section requires the knowledge of the intensity distribution of the ground-state transitions and their branching ratios. As these cannot be derived directly from the measured spectra, we applied statistical methods to discriminate between γ rays from nuclear excitations and photons scattered by atomic processes and to disentangle the intensity distributions of elastic and inelastic transitions in the quasicontinuum of nuclear levels.

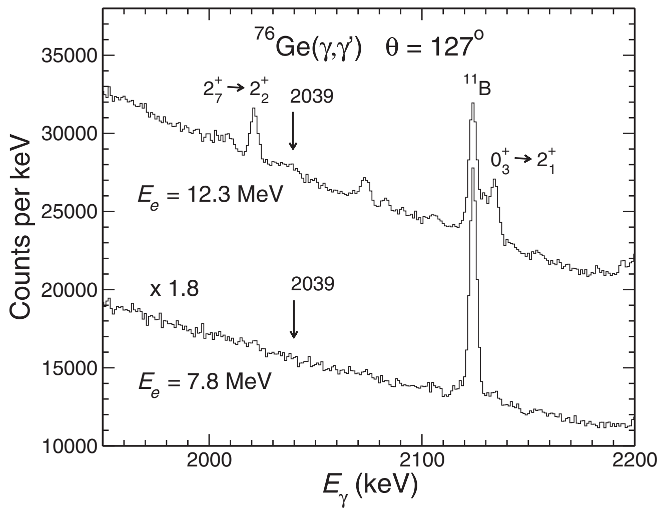

FIG. 3. Parts of spectra measured at $E_e = 7.8$ MeV (bottom) and $E_e = 12.3$ MeV (top) showing the energy section around the expected 2039-keV signal. Note that the 7.8-MeV spectrum was scaled up by a factor of 1.8 to make the two spectra better comparable. The labels $2_7^+ \rightarrow 2_2^+$ and $0_3^+ \rightarrow 2_1^+$ mark the corresponding transitions in ^{76}Ge, 2039 is the energy of the $0\nu\beta\beta$ signal and ^{11}B denotes a transition in this nuclide.

First, a spectrum of the ambient background adjusted to the intensities of the transitions from ^{40}K and ^{208}Tl decay in the in-beam spectrum was subtracted from the measured spectrum. To correct the measured spectrum for the detector response, spectra of monoenergetic γ rays were calculated in steps of 10 keV by using the simulation code GEANT4. Starting from the high-energy end of the experimental spectrum, the simulated spectra were subtracted sequentially (spectrum-stripping method [46]).

The background radiation produced by atomic processes in the ^{76}Ge target was obtained from a GEANT4 simulation. The simulation contains the detector crystals and housings, the BGO shields, the beam tube, and detector shielding. Because of not including other components such as detector stands, cooling systems, etc., one cannot expect a perfect description, in particular not at low energies in the intense region of backscattering and annihilation peaks. This is, however, not critical for the determination of the cross sections at higher energy as described in the following. The atomic background at $E_e = 7.8$ MeV was derived from the atomic background simulated for $E_e = 12.3$ MeV by unfolding with the corresponding flux and folding with the flux at $E_e = 7.8$ MeV to save computing time. The calculated atomic backgrounds are compared with the response-corrected spectra at $E_e = 7.8$ MeV in Fig. 4 and at $E_e = 12.3$ MeV in Fig. 5. The atomic background amounts in average to only a few percent of the intensity in the spectrum, but coincides with that above the neutron threshold, which proves the right magnitude. This behavior is similar to that found in previous studies [36,47–53] and shows that the experimental spectrum contains a considerable amount of nuclear strength in a quasicontinuum. This is

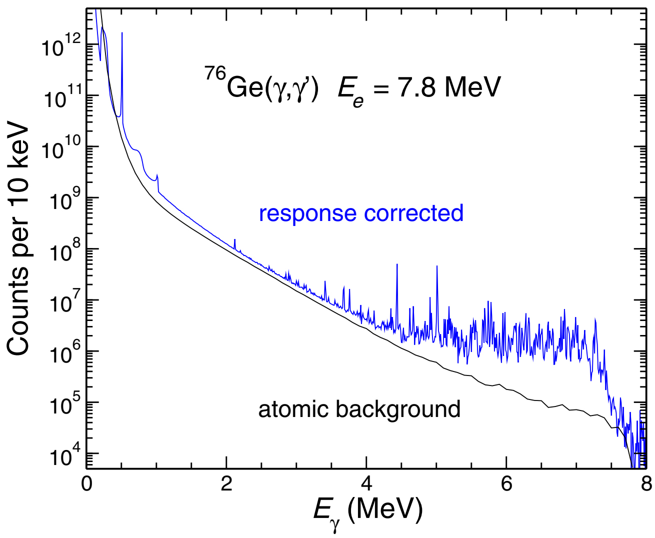

FIG. 4. Spectrum of the two detectors at 127° and $E_e = 7.8$ MeV, corrected for detector response (blue), and simulated spectrum of photons scattered from the target to the detectors by atomic processes (black).

formed by a large number of unresolved transitions with small intensities that are the result of the increasing nuclear level density at high energy in combination with the finite detector resolution. Because of the different orders of magnitude, the nuclear intensity distribution resulting from the subtraction of the simulated atomic background is not very sensitive to uncertainties of the latter, for which we assume 5%. The nuclear intensity distribution contains ground-state (elastic) transitions and, in addition, branching (inelastic) transitions to lower lying excited states as well as transitions from those states to the ground state (cascade transitions). The different

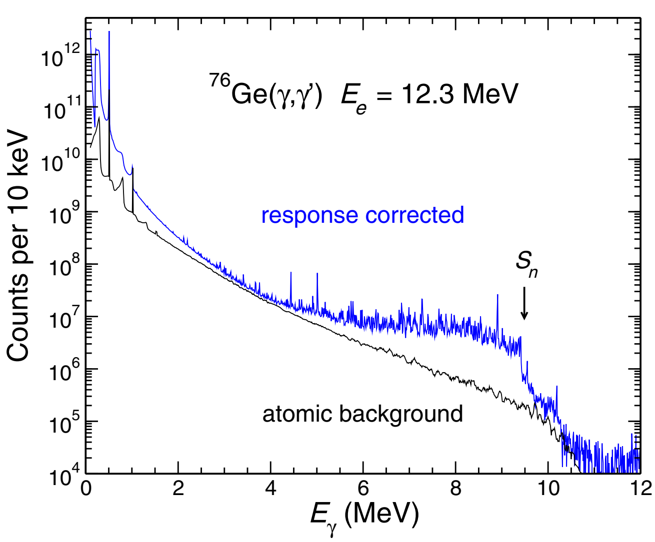

FIG. 5. Spectrum of the two detectors at 127° and $E_e = 12.3$ MeV corrected for detector response (blue), and simulated spectrum of photons scattered from the target to the detectors by atomic processes (black).

types of transitions cannot be clearly distinguished. However, for the determination of the photoabsorption cross section and the partial widths Γ_0, the intensities of the ground-state transitions are needed. Therefore, contributions of inelastic and cascade transitions have to be subtracted from the spectra. We corrected the intensity distributions by simulating γ-ray cascades from the levels in the entire energy region using the code γDEX [37,54]. This code works analogously to the strategy of the code DICEBOX [55] developed for (n,γ) reactions, but in addition it includes also the excitation from the ground state. In the present simulations, level schemes (nuclear realizations) including states with $J = 0,..., 5$ were created for energy bins of 10 keV, which describe statistical averages for a number of states in the bins resulting from calculated level densities. Below about 3 MeV, where the level density is too low for the statistical approach, known low-lying levels were taken into account by filling the respective bins and deriving the level density from the number of levels in a bin. The level densities in the statistical region at higher energy were calculated by using the constant-temperature model [56] with the parameters $T = 0.92(1)$ MeV and $E_0 = 0.13(5)$ MeV adjusted to experimental level densities [57]. In the individual nuclear realizations, the values of T and E_0 were varied randomly within a Gaussian distribution with a standard deviation corresponding to the uncertainties given in Ref. [57]. The parity distribution of the level densities was modeled according to the information given in Ref. [58]. Partial widths were varied in the individual nuclear realizations applying the Porter-Thomas distribution [59].

The first inputs for the photon strength function simulations were assumed to be Lorentz shaped. For the $E1$ strength, a sum of three Lorentz functions (TLO) that account for a triaxial deformation of the nucleus was used with parameters described in Refs. [60,61]. In the present case, deformation parameters of $\beta_2 = 0.26$ [62] and $\gamma = 26^\circ$ [63] were applied. The parameters for the $M1$ and $E2$ strengths were taken from global parametrizations of $M1$ spin-flip resonances and $E2$ isoscalar resonances, respectively [64]. Low-lying levels were also taken into account. Spectra of γ-ray cascades were generated for groups of levels in energy bins of $\Delta E = 100$ keV. Starting from the high-energy end of the intensity distribution, that contains ground-state transitions only, the simulated intensities of the ground-state transitions were normalized to the experimental ones in the considered bin. The intensity distribution of the branching transitions was subtracted from the total intensity distribution. Applying this procedure step by step for each energy bin moving toward the low-energy end of the spectrum, one obtains the intensity distribution of the ground-state transitions. Simultaneously, the branching ratios $b_0(E)$ of the ground-state transitions are determined for each energy bin. In an individual nuclear realization, the branching ratio $b_0(E)$ is calculated as the ratio of the sum of the intensities of the ground-state transitions from all levels in ΔE to the total intensity of all transitions depopulating those levels to either any low-lying energy bin or to the ground state [37,47,48,50,54,65]. Branching ratios $\langle b_0(E)\rangle$, averaged over the many nuclear realizations in the present cascade simulations, are illustrated in Fig. 6.

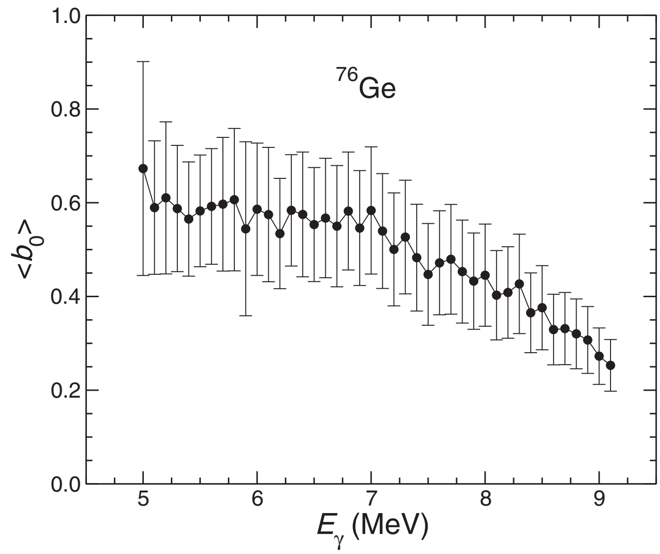

FIG. 6. Average branching ratios of ground-state transitions resulting from the simulations of statistical γ-ray cascades up to S_n as described in the text.

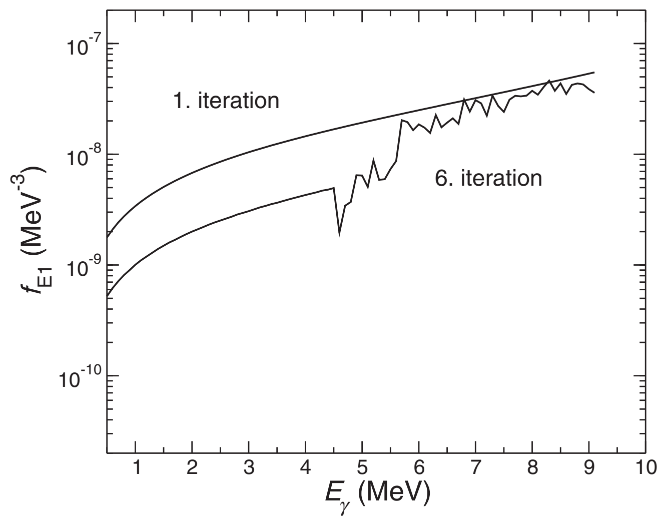

FIG. 7. $E1$ strength functions used as inputs for the first and sixth iteration steps of the γ-ray cascade simulations. See text for details.

The uncertainty of the number of counts $N(E)$ in an energy bin of the experimental intensity distribution was deduced as

$$\delta N(E) = \sqrt{N(E)} + \sum_{E'} [\sqrt{N(E' > E)}\, b(E' \to E)], \quad (3)$$

where $b(E' \to E)$ is the branching intensity from bin E' to bin E. We transform $N(E)$ to the scattering cross section according to

$$\sigma_{\gamma\gamma}(E) = N(E)/[\epsilon(E)\, \Phi_\gamma(E)\, W(E)\, N_N\, \Delta t\, \Delta E\,] \quad (4)$$

with the quantities defined in Eq. (1), the absolute detector efficiency $\epsilon(E)$, the measuring time Δt, and the bin width ΔE. The absorption cross section in each bin is obtained as $\sigma_\gamma(E) = \sigma_{\gamma\gamma}(E)/b_0(E)$ for each nuclear realization. Finally, the absorption cross sections of each bin were obtained by averaging over the values of the individual nuclear realizations.

The simulations were performed iteratively, where the strength function obtained from an iteration step was used as the input for the next step. We note that the simulations are little sensitive to the shape of the first input strength function, which was tested, for example, in Refs. [44,54]. The iteration is stopped when the input strength function and the output strength function were in agreement within their respective uncertainties. This was achieved after the sixth iteration in the present case for $E_e = 12.3$ MeV. Toward low energy, the uncertainties increase due to the use of the spectrum-stripping method and the strength functions do not converge. Besides, the assumption of a statistical quasicontinuum becomes invalid and individual states become important. Therefore, the low-energy parts of the strength functions obtained from the individual iteration steps were replaced by the mentioned Lorentz curves as soon as the uncertainties of the values exceed 100%, and the combination of the Lorentz curve at low energy and the data at high energy resulting from the iteration was used as the input strength function for the next iteration step. For illustration, the input strength functions used for the first and sixth iteration steps in the analysis of the experiment at $E_e = 12.3$ MeV are shown in Fig. 7. As a consequence of the described issues, the cross sections cannot be determined reliably below about 6 MeV. The procedure just described was also performed for the measurement at $E_e = 7.8$ MeV to extend the cross-section data to low excitation energy. We note that the methods described here were tested in several ways. In combined studies using (γ, γ') and (n, γ) reactions, the strength functions obtained from the (γ, γ') experiments were used as inputs for the analysis of the (n, γ) data and gave a consistent description [54,66,67]. The calculated branching ratios $\langle b_0(E)\rangle$ proved to be compatible with experimental values obtained from experiments with quasimonoenergetic photon beams [37,49].

The final absorption cross sections as obtained from the last iteration steps are listed in Table II and graphed in Fig. 8. The uncertainties of the cross-section values include statistical uncertainties of the spectrum, the given uncertainties of the efficiency and the subtracted simulated background spectrum, uncertainties of the flux resulting from the integrated cross sections of the ^{11}B levels, and the uncertainties of the level-density parameters given in the text above. Systematic uncertainties of level-density models can result in additional uncertainties of up to about 20%, which are not included here. These deviations of modeled from experimentally determined level densities and between the various level-density models are, for example, discussed for the case of ^{76}Ge in Ref. [69].

IV. DISCUSSION

The photoabsorption cross section resulting from the present experiments is compared with the cross section of the (γ, n) reaction [68] in Fig. 8. In addition, the TLO with the deformation parameters given in Sec. III and the photoabsorption cross section given in the latest TALYS-based evaluated nuclear data library (TENDL-2019) [70] are displayed. In the latter, the standard Lorentzian (Brink-Axel model) [13,71,72]

TABLE II. Photoabsorption cross section of ^{76}Ge deduced from the present (γ,γ') experiments at $E_e = 7.8$ MeV and $E_e = 12.3$ MeV.

	σ (mb)[a]	
E_γ (MeV)	$E_e = 7.8$ MeV	$E_e = 12.3$ MeV
5.0	0.18(3)	
5.1	0.18(5)	
5.2	0.28(7)	
5.3	0.33(7)	
5.4	0.28(7)	
5.5	0.25(5)	
5.6	0.30(5)	
5.7	0.66(12)	
5.8	0.87(15)	
5.9	0.62(10)	
6.0	0.70(13)	2.2(12)
6.1	0.79(12)	1.8(8)
6.2	0.70(10)	1.9(8)
6.3	1.36(22)	2.7(9)
6.4	1.48(23)	2.2(5)
6.5	1.00(13)	2.7(6)
6.6	1.62(21)	3.0(4)
6.7	1.93(27)	2.8(3)
6.8	2.9(4)	4.5(3)
6.9	3.3(4)	3.7(3)
7.0	2.9(3)	4.7(3)
7.1	3.8(4)	4.8(3)
7.2	3.8(4)	4.1(2)
7.3	3.9(4)	5.4(3)
7.4	4.4(4)	5.1(3)
7.5	2.51(26)	4.9(3)
7.6		5.8(3)
7.7		6.5(3)
7.8		6.5(3)
7.9		6.9(3)
8.0		7.6(4)
8.1		7.1(3)
8.2		8.2(4)
8.3		9.2(4)
8.4		8.0(4)
8.5		9.2(4)
8.6		8.0(4)
8.7		8.6(4)
8.8		8.7(4)
8.9		9.9(5)
9.0		8.3(4)
9.1		8.1(4)
9.2		8.2(4)
9.3		9.2(5)
9.4		9.1(5)
9.5		4.7(3)
9.6		1.93(9)
9.7		0.92(4)
9.8		0.88(4)
9.9		0.72(3)
10.0		0.74(3)

[a]Absorption cross section resulting from the experimental intensity distribution including the quasicontinuum, corrected for branching intensities and branching ratios obtained from γ-ray cascade simulations. The uncertainties include statistical uncertainties of the spectra (see Sec. III), the given uncertainties of the efficiencies and the subtracted simulated background spectra, uncertainties of the flux resulting from the integrated cross sections of the ^{11}B levels, and the given uncertainties of the level-density parameters.

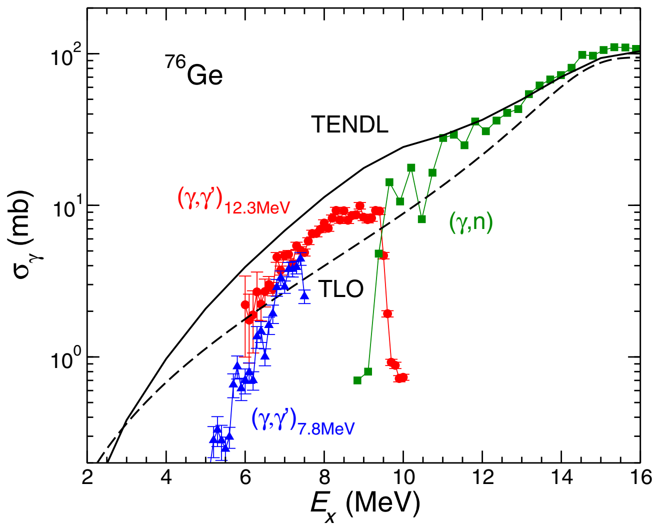

FIG. 8. Photoabsorption cross sections of ^{76}Ge resulting from the present (γ,γ') experiments at $E_e = 7.8$ MeV (blue triangles) and at $E_e = 12.3$ MeV (red circles), from (γ,n) data (green squares) taken from Ref. [68], from calculations using the TALYS code as given in the TENDL-2019 library (black solid curve), and from the TLO with deformation parameters given in the text (black dashed curve).

was used as a strength function in the (γ,γ') reaction [73]. The present (γ,γ') cross section shows extra strength above the TLO in the energy region from about 6 MeV to S_n, which is attributed to the PDR. The TENDL cross section is greater than the present one, but also includes a bump in the PDR region in contrast to the TLO. The cross section of ^{76}Ge is compared with those of the neighboring isotope ^{74}Ge [51] and of the isotone ^{78}Se [52,54] resulting from analogous experiments and methods in Fig. 9. In the PDR region from

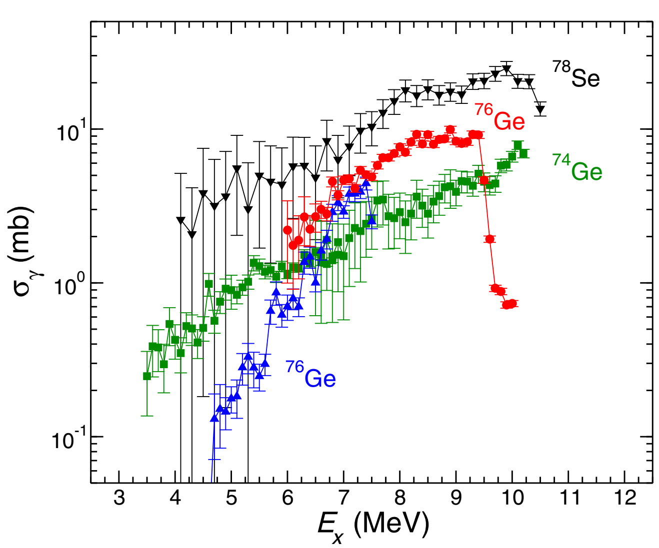

FIG. 9. Photoabsorption cross sections of ^{74}Ge (green squares), ^{76}Ge (blue triangles and red circles), and ^{78}Se (black triangles), resulting from (γ,γ') experiments at γELBE. The data for ^{74}Ge were taken from Ref. [51] and the data for ^{78}Se were taken from Refs. [52,54].

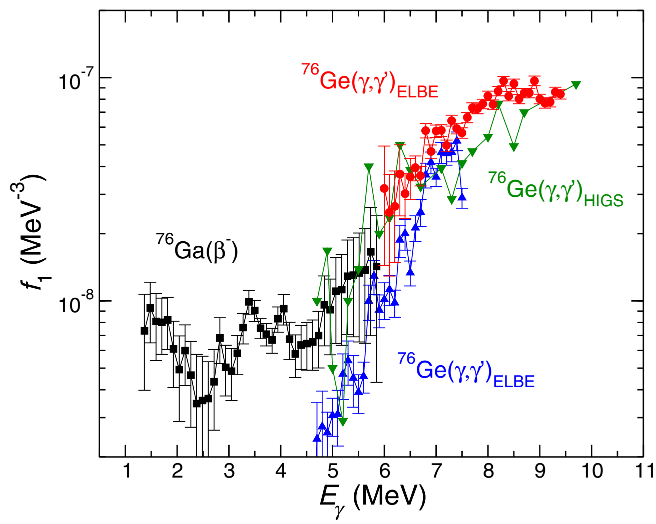

FIG. 10. Photon strength functions for ^{76}Ge from the present (γ,γ') experiment (blue triangles and red circles), from β decay of ^{76}Ga (black squares), taken from Ref. [27], and from a (γ,γ') experiment at HIγS (green triangles), taken from Ref. [28].

about 6 to 9 MeV, the cross section of ^{76}Ge appears to be in average by a factor of about two higher than that of ^{74}Ge, but by a factor of about two smaller than that of ^{78}Se. Toward low energy, the cross section obtained from the low-energy measurement on ^{76}Ge drops more rapidly than the ones in ^{74}Ge and ^{78}Se. These relatively large differences to nuclides with two neutrons less or two protons more, respectively, are remarkable, and interesting to be tested by nuclear models.

The photon strength function deduced from the present photoabsorption cross section of ^{76}Ge is compared with preliminary results from a (γ,γ') experiment with quasi-monoenergetic photons at the HIγS facility [28] and with data obtained from an experiment applying the so-called Oslo method in connection with the β decay of ^{76}Ga [27] in Fig. 10. The data from the HIγS and the β decay experiments exceed the present data below 6 MeV. Between 7 and 9 MeV, the HIγS data amount in average to about 70% of the present data. They were obtained from an analysis of mainly resolved elastic transitions [74]. This means that average branching ratios $\langle b_0(E)\rangle$ in energy bins are overestimated at high excitation energy and, hence, the photoabsorption cross section is underestimated. Besides, strength in the quasicontinuum was not taken into account in that analysis. Similar discrepancies resulting from missing strength in the quasicontinuum were also reported in other recent studies [52,75,76]. On the other hand, the present $\langle b_0(E)\rangle$ include uncertainties of the inputs for the statistical cascade simulations, for example, of the used level-density model.

Whereas the strength functions deduced from photoabsorption cross sections contain exclusively ground-state transitions from $J = 1$ states, the strength functions obtained from light-ion induced reactions or from β decay comprise a large number of transitions linking many states of various spins up to about $J = 10$, which may cause different characteristics of the strength functions. The strength function of ^{76}Ge from β decay continues to low transition energies that belong to cascade transitions between close-lying levels at high excitation energy. It shows the characteristic upbend below about 2.5 MeV that was also observed in the isotopic neighbors ^{73}Ge and ^{74}Ge [77]. This low-energy enhancement of strength has been described in shell-model calculations as resulting from the large strengths of many $M1$ transitions between states generated by recoupling the spins of protons and neutrons in high-j orbitals [78–80]. Interestingly, a bump appears between about 3 and 4.5 MeV in ^{76}Ge in addition to the low-energy upbend. In the shell-model calculations, such a bump appears in open-shell nuclei and has been related to the scissors resonance, which develops in deformed nuclides [81]. A pronounced bump around 3 MeV in addition to the low-energy upbend was also observed in Sm isotopes [82,83]. The (γ,γ') data principally contain also inelastic and cascade transitions between close-lying states at high excitation energy that contribute to the low-energy enhancement [84]. Those transitions are hidden in the huge background in the low-energy parts of the γ-ray spectra. An identification of the low-energy enhancement in (γ,γ') experiments may be feasible by using an efficient multidetector array and applying coincidence techniques. An intensity estimate for such experiments in connection with monoenergetic photon beams is given in Ref. [84].

V. SUMMARY

The dipole-strength distribution in ^{76}Ge was studied up to the neutron-separation energy in photon-scattering experiments at the γELBE bremsstrahlung facility using two electron energies. A total of 210 levels was identified. Spins $J = 1$ were deduced from angular correlations of ground-state transitions. A γ transition in the region of interest for the $0\nu\beta\beta$ decay has not been observed.

The intensity distribution obtained from the measured spectra was corrected for the detector response and a simulated spectrum of photons scattered from the target by atomic interactions was subtracted. The remaining spectrum contains a continuum part in addition to the resolved peaks, which was included in the determination of the photoabsorption cross section. An assignment of inelastic transitions to particular levels and, thus, the determination of branching ratios was, in general, not possible. Therefore, we performed simulations of statistical γ-ray cascades to estimate intensities of branching transitions. These were subtracted from the experimental intensity distribution and the remaining intensities of ground-state transitions were corrected on average for their branching ratios. In this way, a continuous photoabsorption cross section was derived for the energy range from about 5 MeV up to the neutron threshold at 9.4 MeV.

The absorption cross section of ^{76}Ge displays an extra strength on top of the tail of a Lorentz function for the GDR in the range between 6 and 9 MeV that can be considered as the PDR. The shape of the PDR is relatively smooth and approximated by cross sections calculated in the statistical model as given in the TENDL library. The PDR is more pronounced and by a factor of about two higher in magnitude than in the isotope ^{74}Ge, but on the other hand by a factor of about two smaller than in the isotope ^{78}Se. The strength function of ^{76}Ge resulting from the present work is comparable with the ones from other experiments in the PDR region, but drops rapidly toward small energy.

ACKNOWLEDGMENTS

We thank the operating crew of the ELBE accelerator for the cooperation. R.M. acknowledges support by the U.S. Department of Energy, Office of Science, Office of Nuclear Physics under Grant No. LANLEM78.

[1] K. Zuber, *Neutrino Physics* (CRC Press, Boca Raton, FL, 2020).
[2] S. I. Alvis, I. J. Arnquist, F. T. Avignone, A. S. Barabash, C. J. Barton, V. Basu, F. E. Bertrand, B. Bos, M. Busch, M. Buuck *et al.* (Majorana Collaboration), Phys. Rev. C **100**, 025501 (2019).
[3] M. Agostini, A. M. Bakalyarov, M. Balata, I. Barabanov, L. Baudis, C. Bauer, E. Bellotti, S. Belogurov, A. Bettini, L. Bezrukov *et al.*, Science **365**, 1445 (2019).
[4] M. Agostini, A.M. Bakalyarov, M. Balata, I. Barabanov, L. Baudis, C. Bauer, E. Bellotti, S. Belogurov, A. Bettini, L. Bezrukov *et al.* (GERDA Collaboration), Phys. Rev. Lett. **120**, 132503 (2018).
[5] N. Abgrall, A. Abramov, N. Abrosimov, I. Abt, M. Agostini, M. Agartioglu, A. Ajjaq, S. I. Alvis, F. T. Avignone III, X. Bai *et al.*, in *Workshop on Calculation of Double-Beta-Decay Matrix Elements (MEDEX'17)*, edited by O. Civitarese, I. Stekl, and J. Suhonen, AIP Conf. Proc. No. 1894 (AIP, New York, 2017).
[6] K.-J. Kang, J.-P. Cheng, J. Li, Y.-J. Li, Q. Yue, Y. Bai, Y. Bi, J.-P. Chang, N. Chen 1, N. Chen *et al.*, arXiv:1303.0601.
[7] G. Meierhofer, P. Grabmayr, L. Canella, P. Kudejova, J. Jolie, and N. Warr, Eur. Phys. J. A **48**, 20 (2012).
[8] D. C. Camp and B. P. Foster, Nucl. Phys. A **177**, 401 (1971).
[9] A. Negret, C. Borcea, and A. J. M. Plompen, Phys. Rev. C **88**, 027601 (2013).
[10] S. Mukhopadhyay, B. P. Crider, B. A. Brown, S. F. Ashley, A. Chakraborty, A. Kumar, M. T. McEllistrem, E. E. Peters, F. M. Prados-Estévez, and S. W. Yates, Phys. Rev. C **95**, 014327 (2017).
[11] R. Schwengner, R. Beyer, F. Dönau, E. Grosse, A. Hartmann, A. R. Junghans, S. Mallion, G. Rusev, K. D. Schilling, W. Schulze, and A. Wagner, Nucl. Instrum. Methods Phys. Res., Sect. A **555**, 211 (2005).
[12] S. Goriely, P. Dimitriou, M. Wiedeking, T. Belgya, R. Firestone, J. Kopecky, M. Krtiĉka, V. Plujko, R. Schwengner, S. Siem, H. Utsunomiya, S. Hilaire, S. Péru, Y. S. Cho, D. M. Filipescu, N. Iwamoto, T. Kawano, V. Varlamov, and R. Xu, Eur. Phys. J. A **55**, 172 (2019).
[13] T. Kawano, Y. S. Cho, P. Dimitriou, D. Filipescu, N. Iwamoto, V. Plujko, X. Tao, H. Utsunomiya, V. Varlamov, R. Xu, R. Capote, I. Gheorghe, O. Gorbachenko, Y.L. Jin, T. Renstrøm, K. Stopani, Y. Tian, G. M. Tveten, J. M. Wang, T. Belgya, R. Firestone, S. Goriely, J. Kopecky, M. Krtiĉka, R. Schwengner, S. Siem, and M. Wiedeking, Nucl. Data Sheets **163**, 109 (2020).
[14] W. Hauser and H. Feshbach, Phys. Rev. **87**, 366 (1952).
[15] G. A. Bartholomew, E. D. Earle, A. J. Ferguson, J. W. Knowles, and M. A. Lone, in *Advances in Nuclear Physics*, edited by M. Baranger and E. Vogt (Springer, Boston, MA, 1973), Vol. 7, pp. 229–324.
[16] D. Savran, T. Aumann, and A. Zilges, Prog. Part. Nucl. Phys. **70**, 210 (2013).
[17] A. Bracco, E. G. Lanza, and A. Tamii, Prog. Part. Nucl. Phys. **106**, 360 (2019).
[18] M. Beard, S. Frauendorf, B. Kämpfer, R. Schwengner, and M. Wiescher, Phys. Rev. C **85**, 065808 (2012).
[19] N. Tsoneva, S. Goriely, H. Lenske, and R. Schwengner, Phys. Rev. C **91**, 044318 (2015).
[20] M. Arnould, S. Goriely, and K. Takahashi, Phys. Rep. **450**, 97 (2007).
[21] F. Käppeler, R. Gallino, S. Bisterzo, and W. Aoki, Rev. Mod. Phys. **83**, 157 (2011).
[22] A. Jung, S. Lindenstruth, H. Schacht, B. Starck, R. Stock, C. Wesselborg, R. D. Heil, U. Kneissl, J. Margraf, H. H. Pitz, and F. Steiper, Nucl. Phys. A **584**, 103 (1995).
[23] K. Sonnabend, D. Savran, J. Beller, M. A. Büssing, A. Constantinescu, M. Elvers, J. Endres, M. Fritzsche, J. Glorius, J. Hasper, J. Isaak, B. Löher, S. Müller, N. Pietralla, C. Romig, A. Sauerwein, L. Schnorrenberger, C. Wälzlein, A. Zilges, and M. Zweidinger, Nucl. Instrum. Methods Phys. Res., Sect. A **640**, 6 (2011).
[24] H. R. Weller, M. W. Ahmed, H. Gao, W. Tornow, Y. K. Wu, M. Gai, and R. Miskimen, Prog. Part. Nucl. Phys. **62**, 257 (2009).
[25] V. Werner, N. Cooper, P. M. Goddard, P. Humby, R. S. Ilieva, G. Rusev, J. Beller, C. Bernards, B. P. Crider, J. Isaak *et al.*, EPJ Web Conf. **93**, 01031 (2015).
[26] N. M. Cooper, Ph.D. dissertation, Yale University, New Haven, CT, 2015 (unpublished).
[27] A. Spyrou, S. N. Liddick, A. C. Larsen, M. Guttormsen, K. Cooper, A. C. Dombos, D. J. Morrissey, F. Naqvi, G. Perdikakis, S. J. Quinn, T. Renstrom, J. A. Rodriguez, A. Simon, C. S. Sumithrarachchi, and R. G. T. Zegers, Phys. Rev. Lett. **113**, 232502 (2014).
[28] A. P. Tonchev, J. E. Escher, N. Scielzo, P. Bedrossian, R. S. Ilieva, P. Humby, N. Cooper, P. M. Goddard, V. Werner, W. Tornow *et al.*, EPJ Web Conf. **146**, 01013 (2017).
[29] F. Ajzenberg-Selove, Nucl. Phys. A **506**, 1 (1990).
[30] G. Rusev, A. P. Tonchev, R. Schwengner, C. Sun, W. Tornow, and Y. K. Wu, Phys. Rev. C **79**, 047601 (2009).
[31] G. Rusev, Ph.D. dissertation, Technische Universität Dresden, Dresden, Germany, 2007, Report FZD-478 [http://www.hzdr.de/publications/010008/10008.pdf].
[32] S. Agostinelli, J. Allison, K. Amako, J. Apostolakis, H. Araujo, P. Arce, M. Asai, D. Axen, S. Banerjee, G. Barrand, F. Behne *et al.*, Nucl. Instrum. Methods Phys. Res., Sect. A **506**, 250 (2003).
[33] J. Allison, K. Amako, J. Apostolakis, H. Araujo, P. Arce Dubois, M. Asai, G. Barrand, R. Capra, S. Chauvie, R. Chytracek *et al.*, IEEE Trans. Nucl. Sci. **53**, 270 (2006).
[34] J. Allison, K. Amako, J. Apostolakis, P. Arce, M. Asai, T. Aso, E. Bagli, A. Bagulya, S. Banerjee, G. Barrand *et al.*, Nucl. Instrum. Methods Phys. Res. A **835**, 186 (2016).
[35] R. Schwengner, G. Rusev, N. Benouaret, R. Beyer, M. Erhard, E. Grosse, A. R. Junghans, J. Klug, K. Kosev, L. Kostov, C. Nair, N. Nankov, K. D. Schilling, and A. Wagner, Phys. Rev. C **76**, 034321 (2007).

[36] G. Rusev, R. Schwengner, F. Dönau, M. Erhard, E. Grosse, A.R. Junghans, K. Kosev, K. D. Schilling, A. Wagner, F. Bečvár, and M. Krtička, Phys. Rev. C **77**, 064321 (2008).
[37] R. Massarczyk, R. Schwengner, F. Dönau, E. Litvinova, G. Rusev, R. Beyer, R. Hannaske, A. R. Junghans, M. Kempe, J. H. Kelley, T. Kögler, K. Kosev, E. Kwan, M. Marta, A. Matic, C. Nair, R. Raut, K. D. Schilling, G. Schramm, D. Stach, A. P. Tonchev, W. Tornow, E. Trompler, A. Wagner, and D. Yakorev, Phys. Rev. C **86**, 014319 (2012).
[38] M. Marta, E. Trompler, D. Bemmerer, R. Beyer, C. Broggini, A. Caciolli, M. Erhard, Z. Fülöp, E. Grosse, G. Gyurky, R. Hannaske, A. R. Junghans, R. Menegazzo, C. Nair, R. Schwengner, T. Szücs, S. Vezzu, A. Wagner, and D. Yakorev, Phys. Rev. C **81**, 055807 (2010).
[39] E. Trompler, Diploma thesis, Technische Universität Dresden, Dresden, Germany, 2009, Report No. FZD-523, http://www.hzdr.de/publications/013364/13364.pdf.
[40] S. Carson, C. Iliadis, J. Cesaratto, A. Champagne, L. Downen, M. Ivanovic, J. Kelley, R. Longland, J. R. Newton, G. Rusev, and A. P. Tonchev, Nucl. Instrum. Method A **618**, 190 (2010).
[41] E. Haug, Radiat. Phys. Chem. **77**, 207 (2008).
[42] G. Roche, C. Ducos, and J. Proriol, Phys. Rev. A **5**, 2403 (1972).
[43] F. Salvat, J. D. Martinez, R. Mayol, and J. Parellada, Phys. Rev. A **36**, 467 (1987).
[44] R. Schwengner, G. Rusev, N. Tsoneva, N. Benouaret, R. Beyer, M. Erhard, E. Grosse, A. R. Junghans, J. Klug, K. Kosev, H. Lenske, C. Nair, K. D. Schilling, and A. Wagner, Phys. Rev. C **78**, 064314 (2008).
[45] N. Benouaret, R. Schwengner, G. Rusev, F. Dönau, R. Beyer, M. Erhard, E. Grosse, A. R. Junghans, K. Kosev, C. Nair, K. D. Schilling, A. Wagner, and N. Bendjaballah, Phys. Rev. C **79**, 014303 (2009).
[46] A. K. Furr, E. L. Robinson, and C. H. Robins, Nucl. Instrum. Methods **63**, 205 (1968).
[47] G. Rusev, R. Schwengner, R. Beyer, M. Erhard, E. Grosse, A. R. Junghans, K. Kosev, C. Nair, K. D. Schilling, A. Wagner, F. Dönau, and S. Frauendorf, Phys. Rev. C **79**, 061302(R) (2009).
[48] R. Schwengner, R. Massarczyk, G. Rusev, N. Tsoneva, D. Bemmerer, R. Beyer, R. Hannaske, A. R. Junghans, J. H. Kelley, E. Kwan, H. Lenske, M. Marta, R. Raut, K. D. Schilling, A. Tonchev, W. Tornow, and A. Wagner, Phys. Rev. C **87**, 024306 (2013).
[49] R. Massarczyk, G. Rusev, R. Schwengner, F. Dönau, C. Bhatia, M. E. Gooden, J. H. Kelley, A. P. Tonchev, and W. Tornow, Phys. Rev. C **90**, 054310 (2014).
[50] A. Makinaga, R. Massarczyk, R. Schwengner, M. Beard, F. Dönau, M. Anders, D. Bemmerer, R. Beyer, R. Hannaske, A. R. Junghans, M. Kempe, T. Kögler, M. Röder, K. Schmidt, and A. Wagner, Phys. Rev. C **90**, 044301 (2014).
[51] R. Massarczyk, R. Schwengner, L. A. Bernstein, M. Anders, D. Bemmerer, R. Beyer, Z. Elekes, R. Hannaske, A. R. Junghans, T. Kögler, M. Röder, K. Schmidt, A. Wagner, and L. Wagner, Phys. Rev. C **92**, 044309 (2015).
[52] A. Makinaga, R. Massarczyk, M. Beard, R. Schwengner, H. Otsu, T. Al-Abdullah, M. Anders, D. Bemmerer, R. Hannaske, R. John, A. R. Junghans, S. E. Müller, M. Röder, K. Schmidt, and A. Wagner, Phys. Rev. C **94**, 044304 (2016).
[53] T. Shizuma, N. Iwamoto, A. Makinaga, R. Massarczyk, R. Schwengner, R. Beyer, D. Bemmerer, M. Dietz, A. Junghans, T. Kögler, F. Ludwig, S. Reinicke, S. Schulz, S. Urlass, and A. Wagner, Phys. Rev. C **98**, 064317 (2018).
[54] G. Schramm, R. Massarczyk, A. R. Junghans, T. Belgya, R. Beyer, E. Birgersson, E. Grosse, M. Kempe, Z. Kis, K. Kosev, M. Krtiĉka, A. Matic, K. D. Schilling, R. Schwengner, L. Szentmiklósi, A. Wagner, and J. L. Weil, Phys. Rev. C **85**, 014311 (2012).
[55] F. Bečvář, Nucl. Instrum. Meth. Sect. A **417**, 434 (1998).
[56] A. Gilbert and A. G. W. Cameron, Can. J. Phys. **43**, 1446 (1965).
[57] T. von Egidy and D. Bucurescu, Phys. Rev. C **80**, 054310 (2009).
[58] S. I. Al-Quraishi, S. M. Grimes, T. N. Massey, and D. A. Resler, Phys. Rev. C **67**, 015803 (2003).
[59] C. E. Porter and R. G. Thomas, Phys. Rev. **104**, 483 (1956).
[60] A. R. Junghans, G. Rusev, R. Schwengner, A. Wagner, and E. Grosse, Phys. Lett. B **670**, 200 (2008).
[61] E. Grosse, A. R. Junghans, and R. Massarczyk, Eur. Phys. J. A **53**, 225 (2017).
[62] S. Raman, C. W. Nestor, Jr., and P. Tikkanen, At. Data Nucl. Data Tables **78**, 128 (2001).
[63] J.-P. Delaroche, M. Girod, J. Libert, H. Goutte, S. Hilaire, S. Péru, N. Pillet, and G. F. Bertsch, Phys. Rev. C **81**, 014303 (2010).
[64] R. Capote, M. Herman, P. Oblozinsky, P. G. Young, S. Goriely, T. Belgya, A. V. Ignatyuk, A. J. Koning, S. Hilaire, V. A. Plujko *et al.*, Nucl. Data Sheets **110**, 3107 (2009).
[65] R. Massarczyk, R. Schwengner, F. Dönau, S. Frauendorf, M. Anders, D. Bemmerer, R. Beyer, C. Bhatia, E. Birgersson, M. Butterling, Z. Elekes, A. Ferrari, M. E. Gooden, R. Hannaske, A. R. Junghans, M. Kempe, J. H. Kelley, T. Kögler, A. Matic, M. L. Menzel, S. Müller, T. P. Reinhardt, M. Röder, G. Rusev, K. D. Schilling, K. Schmidt, G. Schramm, A. P. Tonchev, W. Tornow, and A. Wagner, Phys. Rev. Lett. **112**, 072501 (2014).
[66] R. Massarczyk, G. Schramm, A.R. Junghans, R. Schwengner, M. Anders, T. Belgya, R. Beyer, E. Birgersson, A. Ferrari, E. Grosse, R. Hannaske, Z. Kis, T. Kögler, K. Kosev, M. Marta, L. Szentmiklósi, A. Wagner, and J. L. Weil, Phys. Rev. C **87**, 044306 (2013).
[67] R. Massarczyk, G. Schramm, T. Belgya, R. Schwengner, R. Beyer, D. Bemmerer, Z. Elekes, E. Grosse, R. Hannaske, A. R. Junghans, Z. Kis, T. Kögler, C. Lorenz, K. Schmidt, L. Szentmiklósi, A. Wagner, and J. L. Weil, Phys. Rev. C **93**, 014301 (2016).
[68] P. Carlos, H. Beil, R. Bergère, J. Fagot, A. Leprêtre, A. Veyssière, and G. V. Solodukhov, Nucl. Phys. A **258**, 365 (1976).
[69] A. V. Voinov, T. Renstrøm, D. L. Bleuel, S. M. Grimes, M. Guttormsen, A. C. Larsen, S. N. Liddick, G. Perdikakis, A. Spyrou, S. Akhtar, N. Alanazi, K. Brandenburg, C. R. Brune, T. W. Danley, S. Dhakal, P. Gastis, R. Giri, T. N. Massey, Z. Meisel, S. Nikas, S. N. Paneru, C. E. Parker, and A. L. Richard, Phys. Rev. C **99**, 054609 (2019).
[70] A. J. Koning, D. Rochman, J. Sublet, N. Dzysiuk, M. Fleming, and S. van der Marck, Nucl. Data Sheets **155**, 1 (2019).
[71] D. M. Brink, Ph.D. thesis, Oxford University, Oxford, UK, 1955 (unpublished).
[72] P. Axel, Phys. Rev. **126**, 671 (1962).
[73] A. Koning (private communication).
[74] A. P. Tonchev (private communication).

[75] M. Müscher, J. Wilhelmy, R. Massarczyk, R. Schwengner, M. Grieger, J. Isaak, A. R. Junghans, T. Kögler, F. Ludwig, D. Savran, D. Symochko, M. P. Takacs, M. Tamkas, A. Wagner, and A. Zilges, Phys. Rev. C **102**, 014317 (2020).

[76] J. Wilhelmy, M. Müscher, G. Rusev, R. Schwengner, R. Beyer, M. Bhike, P. Erbacher, F. Fiedler, U. Friman-Gayer, J. Glorius, R. Greifenhagen, S. Hammer, T. Hensel, J. Isaak, A. R. Junghans, Krishichayan, B. Löher, S. E. Müller, N. Pietralla, S. Reinicke, D. Savran, P. Scholz, K. Sonnabend, T. Szücs, M. Tamkas, W. Tornow, S. Turkat, A. Wagner, and A. Zilges, Phys. Rev. C **102**, 044327 (2020).

[77] T. Renstrøm, H. T. Nyhus, H. Utsunomiya, R. Schwengner, S. Goriely, A. C. Larsen, D. M. Filipescu, I. Gheorghe, L. A. Bernstein, D. L. Bleuel, T. Glodariu, A. Görgen, M. Guttormsen, T. W. Hagen, B. V. Kheswa, Y. W. Lui, D. Negi, I. E. Ruud, T. Shima, S. Siem, K. Takahisa, O. Tesileanu, T. G. Tornyi, G. M. Tveten, and M. Wiedeking, Phys. Rev. C **93**, 064302 (2016).

[78] R. Schwengner, S. Frauendorf, and A. C. Larsen, Phys. Rev. Lett. **111**, 232504 (2013).

[79] B. A. Brown and A. C. Larsen, Phys. Rev. Lett. **113**, 252502 (2014).

[80] K. Sieja, Phys. Rev. Lett. **119**, 052502 (2017).

[81] R. Schwengner, S. Frauendorf, and B. A. Brown, Phys. Rev. Lett. **118**, 092502 (2017).

[82] A. Simon, M. Guttormsen, A. C. Larsen, C. W. Beausang, P. Humby, J. T. Harke, R. J. Casperson, R. O. Hughes, T. J. Ross, J. M. Allmond, R. Chyzh, M. Dag, J. Koglin, E. McCleskey, M. McCleskey, S. Ota, and A. Saastamoinen, Phys. Rev. C **93**, 034303 (2016).

[83] F. Naqvi, A. Simon, M. Guttormsen, R. Schwengner, S. Frauendorf, C. S. Reingold, J. T. Burke, N. Cooper, R. O. Hughes, S. Ota, and A. Saastamoinen, Phys. Rev. C **99**, 054331 (2019).

[84] R. Schwengner and G. Rusev, Phys. Rev. C **100**, 054320 (2019).